Braz J Phys (2012) 42:192–206
DOI 10.1007/s13538-012-0066-1

GENERAL AND APPLIED PHYSICS

Aerothermodynamics of Satellite During Atmospheric Reentry for the Whole Range of Gas Rarefaction: Influence of Inelastic Intermolecular Collisions

Dalton Vinicius Kozak · Felix Sharipov

Received: 11 September 2011 / Published online: 29 February 2012

Abstract The aerothermodynamic characteristics of the Brazilian satellite *Satélite de Reentrada Atmosférica* were calculated for orbital-flight and atmospheric-reentry conditions with the direct simulation Monte Carlo method for a diatomic gas. The internal modes of molecule energy in the intermolecular interaction, such as the rotational energy, were taken into account. The numerical calculations cover a range of gas rarefactions wide enough to embrace the free-molecule and hydrodynamic regimes. Two Mach numbers were considered: 10 and 20. Numerical results include the drag force of the satellite, the energy flux, pressure coefficient, and skin friction coefficient over the satellite surface, the density and temperature distributions, and streamlines of the gas flow around the satellite. The influence of the satellite temperature upon these characteristics was evaluated at different satellite temperatures.

Keywords Aerothermodynamics · DSMC · Rarefied gas dynamics · Satellite

1 Introduction

The project of a recoverable satellite must solve two problems concerning rarefied-gas flow. To compute trajectories, one must know the drag forces on the satellite. And to design adequate heat protection, one needs information about the heat flux to the satellite surface. These problems are usually referred to as the aerothermodynamics of space vehicles [1–4].

In the upper levels of the atmosphere, the mean free path of gaseous molecules is of the order of several meters. Under such conditions, the gas flow can be treated as free molecular, i.e., one can neglect the intermolecular collisions to calculate the aerothermodynamic characteristics. The continuum hypothesis is invalid, and the equations of continuum mechanics become inapplicable.

At lower levels of the atmosphere, the satellite speed is still high, in the hypersonic regime, and although the atmosphere can be viewed as a continuum, the continuum equations are still difficult to handle because the density changes around the satellite are so large that regions of rarefied flow can be present [5]. Special treatment is moreover necessary because the molecules can dissociate and recombine in hypersonic flow. One must then turn to the methods of rarefied-gas dynamics, which can be divided in two large groups. In the first group are methods based on the kinetic Boltzmann equation [6–10], while the second group comprises approaches based on the direct simulation Monte Carlo (DSMC) method [11].

While requiring greater computational efforts, the second approach is more suitable for practical applications because the program can be easily generalized to polyatomic gases and gaseous mixtures. This is very important, since in practice one deals with the air, a mixture of polyatomic gases.

The present paper extends the work of Sharipov [12], which was restricted to a monatomic gas. The

D. V. Kozak (✉)
Departamento de Engenharia da Computação,
Pontifícia Universidade Católica do Paraná,
Curitiba, Paraná,Brazil
e-mail: dvkozak@onda.com.br

F. Sharipov
Departamento de Física, Universidade Federal do Paraná
Caixa Postal 19044, Curitiba, 81531-990, Brazil

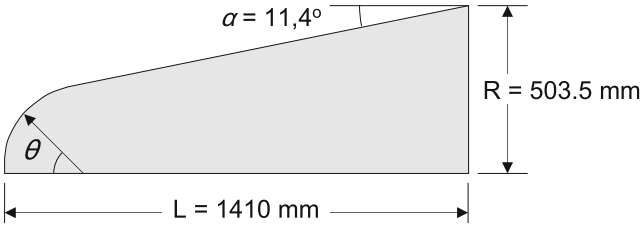

Fig. 1 Shape and dimensions of SARA

DSMC method is here used to calculate the aerothermodynamic characteristics of *Satélite de Reentrada Atmosférica* (SARA). SARA is a Brazilian project of small reusable ballistic reentry satellites, which will be used to realize scientific experiments in microgravity conditions and to deliver results to Earth. The shape of the satellite is presented in Fig. 1.

We want to calculate the drag force, the energy flux to the satellite surface, and the distributions of temperature, density, and local Mach number around the vehicle during orbital flight and atmospheric reentry. The calculations cover the whole range of gas rarefaction, embracing both the free-molecule and hydrodynamic regimes. A diatomic gas is considered, with properties mimicking those of nitrogen. Since energy can be exchanged between the internal degrees of freedom, such as rotational and vibrational molecular modes, and the translational ones, the collisions between particles and between particles and surface are not elastic. This exchange is accounted for in our treatment.

2 Statement of the Problem

The flowfield around the satellite is considered to be axially symmetric. Far upstream from the satellite, the gas velocity U_∞ is parallel to the symmetry axis.

The temperature and density of the unperturbed gas are denoted T_∞ and ρ_∞, respectively. The solution of the problem depends on two principal parameters:

(a) The Mach number, defined as

$$\mathrm{Ma} = \frac{U_\infty}{c}, \quad c = \sqrt{\gamma \frac{kT_\infty}{m}}, \tag{1}$$

where k is the Boltzmann constant, m is the molecular mass, and γ and c are the ratio of specific heats and the speed of sound for the gas, respectively.

(b) The Reynolds number, defined as

$$\mathrm{Re} = \frac{RU_\infty \rho_\infty}{\mu}, \tag{2}$$

where R is the satellite base radius, as indicated in Fig. 1, and μ is the dynamic viscosity of the gas at the temperature T_∞.

The gas rarefaction is characterized by the rarefaction parameter δ, given by

$$\delta = \frac{Rp_\infty}{\mu\, v_\mathrm{m}}, \tag{3}$$

where

$$v_\mathrm{m} = \sqrt{\frac{2kT_\infty}{\mathrm{m}}} \tag{4}$$

is the most probable molecular speed at the temperature T_∞.

Given that $\mu v_\mathrm{m}/p$ is the equivalent free path of gaseous molecules, we see that the rarefaction parameter is inversely proportional to the Knudsen number. The limit $\delta \to 0$ thus corresponds to the free-molecule regime, in which collisions between particles are negligible, and only particle–surface interactions take place. The limit $\delta \to \infty$ corresponds to the hydrodynamic regime, in which interactions between particles are frequent and the continuum hypothesis is valid.

For relatively small pressures, the gases behave like an ideal gas, and the following relation is valid,

$$p_\infty = \rho_\infty RT_\infty = \rho_\infty \frac{k}{m} T_\infty. \tag{5}$$

The combination of (1, 2, 3), and (5) yields the following expression, relating the rarefaction parameter to the ratio between the Mach and Reynolds numbers:

$$\delta = \frac{1}{\sqrt{2\gamma}} \frac{\mathrm{Re}}{\mathrm{Ma}}, \tag{6}$$

which shows that the rarefaction parameter is not an independent variable.

The following macroscopic quantities of practical interest are calculated in the present work.

– *Drag coefficient*

$$C_\mathrm{D} = \frac{F}{p_\mathrm{d} A}, \tag{7}$$

where F is the drag force,

$$p_\mathrm{d} = \frac{1}{2}\rho_\infty U_\infty^2 \tag{8}$$

is the dynamic pressure, and

$$A = \pi R^2 \tag{9}$$

is the satellite frontal area.

– *Energy transfer coefficient*

$$C_\mathrm{h} = \frac{q_\mathrm{n}}{p_\mathrm{d} U_\infty}, \tag{10}$$

where q_n is the energy flux normal to the satellite surface.

– *Pressure coefficient*

$$C_p = \frac{p - p_\infty}{p_d}, \tag{11}$$

where p is the pressure normal to the satellite surface and p_∞ is given by (5).

– *Friction coefficient*

$$C_f = \frac{\tau}{p_d}, \tag{12}$$

where τ is the tangential stress at the satellite surface.

We will calculate these macroscopic quantities as functions of two principal parameters: the Mach number Ma, and the Reynolds number Re.

3 Method

3.1 General Remarks

The DSMC, first proposed by Bird [11], is a statistical technique that describes a gas flow behavior at the molecular level, i.e., at the level of the molecular velocity distribution function. Bird [11] has shown that the DSMC method yields results that are consistent with those obtained from the Boltzmann equation. In essence, the DSMC method simulates the motion of a great number of model particles and their collisions and calculates the macroscopic quantities for each flow cell. A model particle represents a large number of real particles, since the cost of simulating the motion of real particles would rapidly exhaust the resources of any computational center.

First, the coordinates $\boldsymbol{r}_i$ and the velocities $\boldsymbol{v}_i$ of each particle (i = 1, .., N) are stored in computer memory. The flow region is divided into a network of cells, and the time is advanced in time steps Δt, which must be small in comparison with the mean time between two successive collisions.

The motion of particles and the intermolecular collisions are considered separately in each step Δt. The simulation thus amounts to repeating the following processes: (a) free motion of particles without intermolecular collisions and (b) intermolecular collisions without particles motion.

3.2 Free Motion

In this stage, each molecule, with velocity $\boldsymbol{v}_i$, travels a distance during the step Δt. The following expression computes the new coordinate $\boldsymbol{r}_{i,\mathrm{new}}$ from the previous one $\boldsymbol{r}_{i,\mathrm{old}}$

$$\boldsymbol{r}_{i,\mathrm{new}} = \boldsymbol{r}_{i,\mathrm{old}} + \boldsymbol{v}_i \Delta t. \tag{13}$$

If the trajectory of particle crosses a solid surface, then the gas–surface interaction is simulated according to a specific law. In this stage, the differences of momentum, kinetic energy, and internal energy for each particle before and after collision are calculated. These differences are then used to calculate the drag force, pressure coefficient, friction coefficient, and energy transfer coefficient over the entire satellite surface.

We assume the interaction to be diffuse, so that the particles are randomly reflected by the surface in all directions, with equal probabilities. The final velocity is assigned according to a Maxwellian distribution determined by the wall temperature. As shown in [13, 14], only light gases, such as helium, incident on atomically clean surfaces can deviate significantly from diffusive interaction. Since the air comprises gases with molecular masses much greater than helium and since the satellite surface is contaminated during atmospheric reentry, it is an excellent approximation to treat the scattering as diffuse.

After the free motion step, all information concerning particles that have left the flow region is deleted from the computer memory. At the same time, new particles are introduced into the flow region through the boundaries as dictated by the conditions of the unperturbed gas.

3.3 Intermolecular Collisions

3.3.1 Selection of Collision Pairs

The second stage simulates intermolecular collisions. The number of pairs to be selected for collision is calculated from the expression

$$N_{\mathrm{coll}} = \frac{N_p \bar{N}_p F_N (\sigma v_r')_{\max} \Delta t}{2 V_C}, \tag{14}$$

where N_p is the number of particles in the cell at that moment, $\bar{N}_p$ is the average value of N_p until that moment, F_N is the number of real gas particles represented by one model particle, v_r' is the relative speed between the two particles, V_C is the cell volume, and σ is the collision cross-sectional area of the particle.

The probability that two particles collide is proportional to the ratio

$$\frac{\sigma v_r'}{(\sigma v_r')_{\max}}. \tag{15}$$

Given this probability, an acceptance–rejection test selects the pairs that will collide and computes the post-collisional velocities.

The shock cross section of the particles depends on the molecular model. The most common choice is the hard sphere (HS) model, which simplifies the calculations a great deal and calls for no specification of the gas or of its temperature. Here, since we want to investigate the flow of a diatomic gas, like nitrogen, we prefer the variable hard sphere (VHS) model, notice being taken that the required specifications of the gas and of its temperature will restrict the scope of the results.

Accordingly, a pair is accepted for collision when

$$\frac{\sigma v_{\mathrm{r}}'}{(\sigma v_{\mathrm{r}}')_{\max}} > R_{\mathrm{f}}. \tag{16}$$

Here and henceforth R_{f} denotes a random number.

The product $\sigma v_{\mathrm{r}}'$ is obtained from the equality [11]

$$\frac{\sigma v_{\mathrm{r}}'}{\sigma_\infty v_{\mathrm{m}}} = \frac{2^{(\omega-\frac{1}{2})}}{\Gamma(\frac{5}{2}-\omega)} v_{\mathrm{r}}'^{[2(1-\omega)]}, \tag{17}$$

where σ_∞ and v_{m} are reference values for cross-section shock area and most probable molecular speed, respectively, calculated for the temperature T_∞, and ω is the exponent of the temperature in the expression for the viscosity,

$$\mu = \mu_\infty \left(\frac{T}{T_\infty}\right)^{\omega}, \tag{18}$$

where μ_∞ is the viscosity at the temperature T_∞.

3.3.2 Dynamic of Collisions

After the selection and acceptance of the pairs for collision, the post-collisional state of particles must be determined, and to that end, the conservation of energy during the collision must be considered.

For the polyatomic gases studied in this work, the exchange of energy between particles involves not only translational energy but also other modes of energy, such as rotational and vibrational modes. For diatomic gases, in particular, we can consider only two rotational degrees of freedom since the third degree of freedom in the rotational and vibrational modes can be neglected [11].

The conservation of collisional energy for diatomic gases is expressed by the sequence

$$E_{\mathrm{c}} = E_{\mathrm{c}}^* \;\rightarrow\; E_{\mathrm{t}} + E_{\mathrm{r}} = E_{\mathrm{t}}^* + E_{\mathrm{r}}^*, \tag{19}$$

where E_{c} is the pre-collisional energy, which is the total of all energy modes (translational, rotational, and vibrational), and E_{c}^* is the post-collisional energy of the particles; E_{t} is the pre-collisional relative translational energy of the pair of particles and E_{t}^* is the post-collisional relative translational energy of the pair of particles; and E_{r} is the pre-collisional rotational energy and E_{r}^* is the post-collisional rotational energy of the pair of particles.

By contrast with the energy balance in elastic collisions, the relative translational energy changes during an inelastic collision, since there is exchange of energy with the rotational modes. To evaluate the distribution of energy between translational and rotational modes, we refer to the Larsen–Borgnakke model [11]. In the Larsen–Borgnakke model, the post-collisional ratio $E_{\mathrm{t}}/E_{\mathrm{c}}$ for diatomic gases (with two rotational degrees of freedom) follows the distribution function

$$\frac{P(E_{\mathrm{t}}/E_{\mathrm{c}})}{P_{\max}} = \left[\frac{5/2-\omega}{3/2-\omega}\left(\frac{E_{\mathrm{t}}}{E_{\mathrm{c}}}\right)\right]^{3/2-\omega} \times (5/2-\omega)\left(1-\frac{E_{\mathrm{t}}}{E_{\mathrm{c}}}\right). \tag{20}$$

Given this probability distribution and E_{c}^* $(=E_{\mathrm{c}})$, a random value for E_{t}^* is chosen between 0 and E_{c}^* $(E_{\mathrm{t}}^* = R_{\mathrm{f}} E_{\mathrm{c}}^*)$, and the following acceptance–rejection criterion is applied:

$$\frac{P}{P_{\max}} > R_{\mathrm{f}}. \tag{21}$$

Once a E_{t}^* is accepted according to the above criterion, the post-collisional rotational energy of the pair of particles is calculated as

$$E_{\mathrm{r}}^* = E_{\mathrm{c}}^* - E_{\mathrm{t}}^*. \tag{22}$$

The probability distribution for the division of energy between the two particles is uniform. Given two particles, i and j, the post-collisional rotational energies will hence be given by the equalities

$$E_{\mathrm{r}\,i}^* = R_{\mathrm{f}} E_{\mathrm{r}}^*; \quad E_{\mathrm{r}\,j}^* = E_{\mathrm{r}}^* - E_{\mathrm{r}\,i}^*. \tag{23}$$

Section 3.4 shows the thermodynamic temperature to be a function of the translational energy (translational temperature) and the rotational energy (rotational temperature) of the particles in the flow.

The relative speed between the particles after collision is obtained from the equality

$$v_{\mathrm{r}}' = 2\sqrt{\frac{E_{\mathrm{t}}^*}{m}}. \tag{24}$$

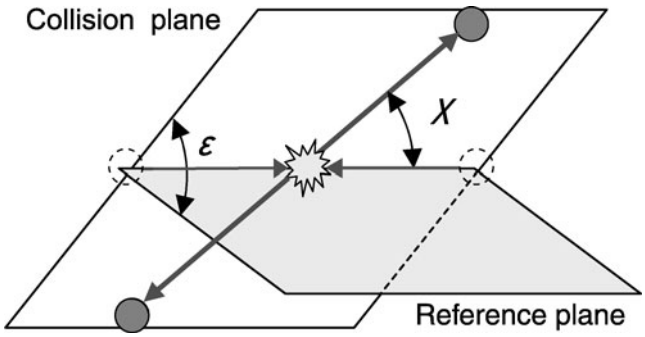

Fig. 2 Collision angles

As shown in Fig. 2, the components of the post-collisional relative velocity can be evaluated from the following expressions:

$$v_{r1} = v'_r \cos\chi, \tag{25}$$

$$v_{r2} = v'_r \sin\chi \cos\epsilon, \tag{26}$$

$$v_{r3} = v'_r \sin\chi \sin\epsilon, \tag{27}$$

where two random numbers, R_f and R'_f, are used to calculate χ and ϵ with the expressions

$$\cos\chi = 2R_f - 1, \quad \epsilon = 2\pi R'_f. \tag{28}$$

The velocity components of particles i and j after collision are

$$v^*_{i\,k} = v_{cmk} + \frac{v'_{rk}}{2}, \quad v^*_{j\,i} = v_{cmk} - \frac{v'_{rk}}{2}, \tag{29}$$

where

$$v_{cmk} = \frac{v_{ik} + v_{jk}}{2}. \tag{30}$$

Here $k = 1, 2, 3$ denotes the axis directions, and the parameter $\boldsymbol{v}_{cm}$ corresponds to the pre-collisional velocity of the center of mass of the pair.

After the collisions have been computed in all cells, the particles move freely during the interval of time Δt, with new or unchanged velocities, depending on whether a collision has or has not occurred, respectively. Another interval of time follows, and all collisional and free motion processes are repeated.

3.3.3 Gas–Surface Interaction

The collision between a particle and the surface is described by a diffuse interaction with complete thermal accommodation. The reflected particle thus has a velocity obeying the Maxwellian distribution at the surface temperature T_s, and its rotational energy is given by the expression [11]

$$E_r^{\,ref} = -kT_s \ln R_f. \tag{31}$$

3.3.4 Relaxation Time

As pointed out by Bird [11], a relaxation time τ defines the delay in the exchange of energy between the translational and the rotational modes. This is the time needed for the deviation of the state function (temperature) to decay to $1/e$ of its initial value as it approaches equilibrium. This time, usually several times larger than the interval between collisions, is given by

$$\tau_R = \frac{Z_R}{\nu}, \tag{32}$$

where τ_R is the rotational relaxation time, Z_R is the rotational relaxation collision number, and ν is the collision frequency.

For the purpose of DSMC simulations, $Z_R = 5$ is generally adopted for nitrogen [15]. To introduce the rotational relaxation time into the computation, one determines the fraction of inelastic collisions during an interaction step. This fraction is given by the parameter X_{inel}, defined as

$$X_{inel} = \frac{1}{Z_R}, \tag{33}$$

In the case of nitrogen, $X_{inel} = 0.2$.

To implement the above procedure, the following test is applied to each pair selected to collide,

$$X_{inel} > R_f. \tag{34}$$

If the inequality (34) holds, the collision is inelastic; otherwise, it is elastic.

3.4 Calculation of Macroscopic Quantities

The macroscopic quantities of practical interest are obtained after sufficiently large time. The density ρ is obtained from the number of particles N_p inside a cell,

$$\rho = \frac{mN_pF_n}{V_C}. \tag{35}$$

The hydrodynamic velocity, i.e., the averaged velocities of particles inside the cell, is calculated as

$$\boldsymbol{u} = \frac{1}{N_p}\sum_{i=1}^{N_p} \boldsymbol{v}_i. \tag{36}$$

The translational temperature is determined by the average kinetic energy of particles in a reference frame moving with the bulk velocity $\boldsymbol{u}$ and is hence calculated as

$$T_t = \frac{2}{3kN_p}\sum_{i=1}^{N_p} \frac{mV_i^2}{2}, \quad \boldsymbol{V}_i = \boldsymbol{v}_i - \boldsymbol{u}. \tag{37}$$

The rotational temperature, directly related to the rotational energy of the particles, is obtained from the equality

$$T_{\mathrm{r}} = \frac{1}{kN_{\mathrm{p}}} \sum_{i=1}^{N_{\mathrm{p}}} E_{\mathrm{r}i}. \tag{38}$$

For monatomic gases, the thermodynamic temperature, or simply the temperature, is evaluated as

$$T = T_{\mathrm{t}}, \tag{39}$$

For diatomic gases, one defines an overall kinetic temperature T_{ov}, given by the expression

$$T_{\mathrm{ov}} = \frac{3T_{\mathrm{t}} + 2T_{\mathrm{r}}}{5}. \tag{40}$$

In thermodynamic equilibrium, $T_{\mathrm{t}} = T_{\mathrm{r}}$. We hence have that

$$T = T_{\mathrm{ov}}. \tag{41}$$

The satellite surface is divided in area segments A_{s}, and the net energy that arrives at an area segment during an interval of time t is given by the equality

$$e_{\mathrm{net}} = \frac{1}{A_{\mathrm{s}}t} \times \sum_{i=1}^{N_{\mathrm{s}}} \left[\frac{m(v_i^{\mathrm{ref}})^2}{2} - \frac{m(v_i^{\mathrm{inc}})^2}{2} + E_{\mathrm{r_i}}^{\mathrm{ref}} - E_{\mathrm{r}i}^{\mathrm{inc}} \right], \tag{42}$$

where $\boldsymbol{v}_i^{\mathrm{inc}}$ is the velocity of particle incident on the surface, $\boldsymbol{v}_i^{\mathrm{ref}}$ is the velocity of particle reflected from the surface, $E_{\mathrm{r}i}^{\mathrm{inc}}$ is the rotational energy of particle incident on the surface, $E_{\mathrm{r}i}^{\mathrm{ref}}$ is the rotational energy of particle reflected from the surface, and t is the time for statistical accumulation.

Since the only mechanism of energy transfer on the satellite surface is due to the molecular collisions, the energy flow is given by the expression

$$\boldsymbol{q}_{\mathrm{n}} = e_{\mathrm{net}}. \tag{43}$$

The coefficients C_{h}, C_{p}, and C_{f} are also obtained from the number of particles N_{s} colliding with each segment during a time interval t.

For the energy transfer coefficient, defined by (10), we have that

$$C_{\mathrm{h}} = \frac{1}{p_{\mathrm{d}}U_\infty} \frac{1}{A_{\mathrm{s}}t} \times \sum_{i=1}^{N_{\mathrm{s}}} \left[\frac{m(v_i^{\mathrm{ref}})^2}{2} - \frac{m(v_i^{\mathrm{inc}})^2}{2} + E_{\mathrm{r}i}^{\mathrm{ref}} - E_{\mathrm{r}i}^{\mathrm{inc}} \right]. \tag{44}$$

For the pressure coefficient, defined by (11), we may write that

$$C_{\mathrm{p}} = \frac{1}{p_{\mathrm{d}}} \left[\frac{1}{A_{\mathrm{s}}t} \sum_{i=1}^{N_{\mathrm{s}}} m(v_{\mathrm{n}i}^{\mathrm{ref}} - v_{\mathrm{n}i}^{\mathrm{inc}}) - p_\infty \right], \tag{45}$$

where $v_{\mathrm{n}i}^{\mathrm{inc}}$ ($v_{\mathrm{n}i}^{\mathrm{ref}}$) is the normal component of the velocity of a particles incident on (reflected from) the surface.

For the friction coefficient, defined by (12), we have that

$$C_{\mathrm{f}} = \frac{1}{p_{\mathrm{d}}} \frac{1}{A_{\mathrm{s}}t} \sum_{i=1}^{N_{\mathrm{s}}} m(v_{\mathrm{t}i}^{\mathrm{ref}} - v_{\mathrm{t}i}^{\mathrm{inc}}), \tag{46}$$

where $v_{\mathrm{t}i}^{\mathrm{inc}}$ ($v_{\mathrm{t}i}^{\mathrm{ref}}$) is the tangential component of the velocity of a particle incident on (reflected from) the surface.

For the drag coefficient, defined by the expression (7), we have the following relation:

$$C_{\mathrm{d}} = \frac{1}{p_{\mathrm{d}}\pi R_{\mathrm{s}}^2} \frac{1}{t} \sum_{i=1}^{N_{\mathrm{s}}} m(v_{xi}^{\mathrm{inc}} - v_{xi}^{\mathrm{ref}}), \tag{47}$$

where v_{xi}^{inc} (v_{xi}^{ref}) is the horizontal component, in the x direction, of the velocity of particle incident on (reflected from) the surface.

3.5 Grid

We lay the cells on a multilevel, regular grid. This arrangement allows finer discretization where the flow properties have larger gradients and in the neighborhood of the satellite surface, to minimize the effect of rectangular grid irregularities.

The region under study has cylindrical symmetry. The radius of the flowfield is three times larger than the radius of the satellite base, and other lengths are defined as shown in Fig. 3. The (linear) dimension of the cells in the neighborhood of the satellite is half the dimension of those far away. Corrections are

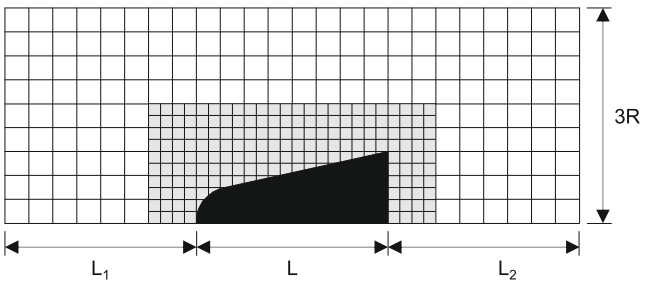

Fig. 3 Grid of cells used in the DSMC code

introduced to account for the smaller volumes of the cells on the surface of the satellite.

3.6 Other Computational Parameters

Model particles are substituted for the much more numerous real particles. The space is discretized in cells of finite size Δr, and the time is discretized in intervals of size Δt. The accuracy of the calculation is expected to improve as the number of model particles approaches the number of real particles and as Δr and Δt shrink in comparison with the mean free path and the mean time between molecular collisions, respectively. Considerations of computational cost imposing constraints on the three parameters, we choose an average number of 2×10^6 model particles, larger cells of size $R/12$, as indicated in Fig. 3, and time increments Δt given by the equality

$$\Delta t = 0.01\, R \left(\frac{m}{2kT_\infty} \right)^{1/2}. \tag{48}$$

Comparison with tests in which the number of particles was doubled, while the cell size and the time increment were halved, has shown that the above parameters limit the numeric uncertainty to about 1% for the drag coefficient and to between 1% and 10% for the other quantities. The computational time necessary to achieve the desired results varied from 2 to 3 days to a month, depending on the Reynolds number.

4 Numerical Results

4.1 General Remarks

The calculations of the flow around the satellite were carried out for the Reynolds numbers ranging from $\mathsf{Re} = 0.1$ to $\mathsf{Re} = 10{,}000$ and for two Mach numbers $\mathsf{Ma} = 10$ to $\mathsf{Ma} = 20$. According to the expression (6), the rarefaction parameter varies from $\delta \approx 0.01$ (free molecule regime) to $\delta \approx 600$ (hydrodynamic regime). These values will represent the typical magnitudes of the Reynolds and Mach numbers during an atmospheric reentry.

Since the satellite is highly heated during a reentry, it is interesting to evaluate the influence of the temperature of satellite surface T_s on the aerothermodynamic characteristics of the satellite. To do this, two values of the temperature ratio T_s/T_∞ were considered: 1 and 10. The first ratio corresponds to a satellite surface at the unperturbed flow temperature, T_∞, i.e., the satellite is "cold." The second value, $T_s/T_\infty = 10$, corresponds to a satellite surface at a considerably higher temperature than the unperturbed flow, i.e., the satellite is "hot." In reality, the surface temperature should vary within the range defined by these two extremes, and the two calculations should reveal the magnitude of the influence of the satellite surface temperature on its aerothermodynamic characteristics.

Table 1 Parameters for monatomic and diatomic gases

Parameter	Gas	
	Monatomic	Diatomic (N_2)
γ	5/3	7/5
ω	0.50	0.74
X_{inel}	0.0	0.2
Molecular interaction	HS	VHS

To evaluate the difference between the monatomic and diatomic gases, both cases were simulated, three parameters being varied as shown in Table 1, where γ is the ratio between specific heats of the gas; ω is the exponent of the viscosity law, defined by (18); and X_{inel} is the parameter defining the fraction of inelastic collisions, as has been explained in Section 3.3.4.

4.2 Drag Coefficient

The drag coefficient, C_D, defined by (7), is shown in Fig. 4 as a function of the Reynolds number, Re; Mach number, Ma; and temperature of the satellite, T_s, for a diatomic gas. The coefficient C_D depends weakly on the Mach number, while it changes significantly with Re in the transition between the free-molecule and hydrodynamic regimes. C_D decays steeply in the interval $10 < \mathsf{Re} < 1{,}000$, the region of Fig. 4 in which the curves are reversed, i.e., in which as Re grows, the $\mathsf{Ma} = 10$ curves sink below the $\mathsf{Ma} = 20$ curves.

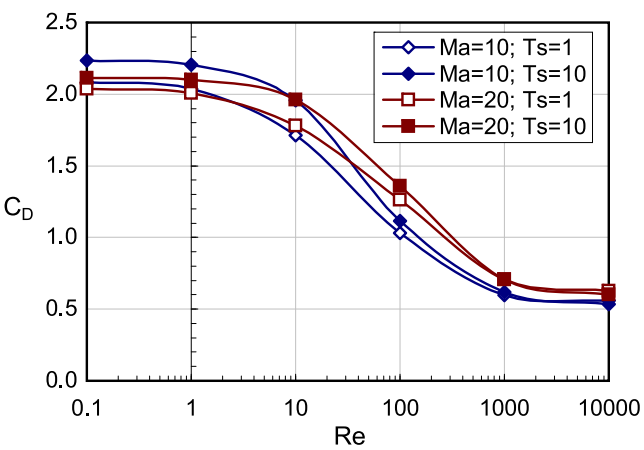

Fig. 4 (Color online) Drag coefficient vs Re for a diatomic gas, N_2

Comparison between the results for the "cold" ($T_s/T_\infty = 1$) and the "hot" ($T_s/T_\infty = 10$) satellites shows that the drag coefficient C_D is most sensitive to the satellite temperature near the free molecules regime, i.e., for $\mathsf{Re} = 0.1$, and for the smaller Mach number in this work, $\mathsf{Ma} = 10$. The change is then close to 9%. The Mach number being larger than 10 under the conditions of satellite reentry, we conclude that the satellite temperature has little influence on the drag coefficient.

As a first approximation, neglecting the small effects of the surface temperature (T_s) and of the Mach number (Ma) on the drag coefficient, we obtained an accurate fit to the data in Fig. 4 with the following expression:

$$C_D = \frac{1.572}{1 + 0.02568\, e^{(2.031\ \log \mathsf{Re})}} + 0.5493. \tag{49}$$

To evaluate the influence of the monatomic gas and diatomic gas hypotheses in the flow simulation, numerical data for C_D are shown in Table 2. At $\mathsf{Ma} = 10$, the drag coefficient of the diatomic gas becomes somewhat smaller than the coefficient of the monatomic gas in the transition region, with a slight inversion after $\mathsf{Re} \approx$ 1,000. These changes are very close to the accuracy of the calculation. At $\mathsf{Ma} = 20$, the difference becomes more noticeable, albeit small. For $\mathsf{Re} > 1{,}000$, the drag coefficient of the diatomic gas is 2–3% smaller than that of the monatomic gas.

4.3 Pressure Coefficient

Figures 5, 6, 7, and 8 display the pressure coefficient C_p for a diatomic gas as a function of the angle θ, defined in Fig. 1, and satellite temperature at Mach 10 and 20, respectively. C_p depends weakly on the Reynolds and

Table 2 Numeric values for drag coefficient, C_D, for monatomic and diatomic (N_2) gases

Ma	Re	Monatomic		Diatomic	
		$\frac{T_s}{T_\infty} = 1$	$\frac{T_s}{T_\infty} = 10$	$\frac{T_s}{T_\infty} = 1$	$\frac{T_s}{T_\infty} = 10$
10	0.1	2.081	2.235	2.081	2.235
	1	2.036	2.207	2.036	2.207
	10	1.718	1.962	1.711	1.958
	100	1.045	1.129	1.031	1.116
	1,000	0.601	0.622	0.596	0.617
	10,000	0.557	0.535	0.561	0.537
	0.1	2.036	2.113	2.036	2.113
	1	2.007	2.099	2.007	2.099
	10	1.780	1.966	1.779	1.963
	100	1.276	1.373	1.262	1.358
	1,000	0.728	0.731	0.705	0.705
	10,000	0.636	0.615	0.627	0.600

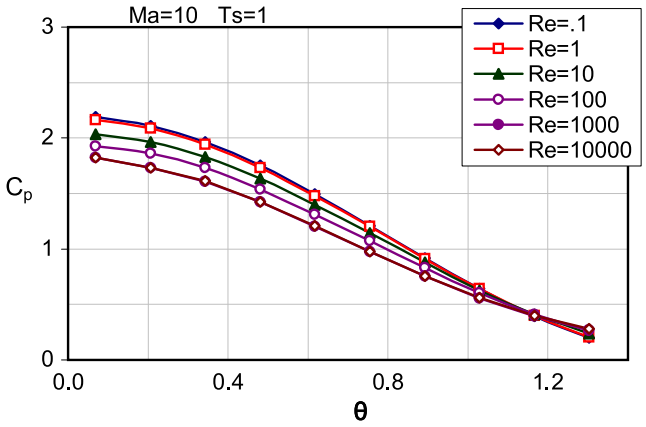

Fig. 5 (Color online) Pressure coefficient at ogive apex for diatomic gas (N_2), $\mathsf{Ma} = 10$, $T_s/T_\infty = 1$

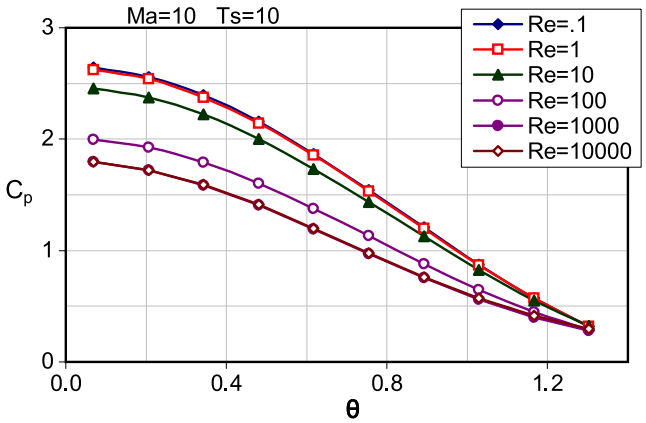

Fig. 6 (Color online) Pressure coefficient at ogive apex for diatomic gas (N_2), $\mathsf{Ma} = 10$, $T_s/T_\infty = 10$

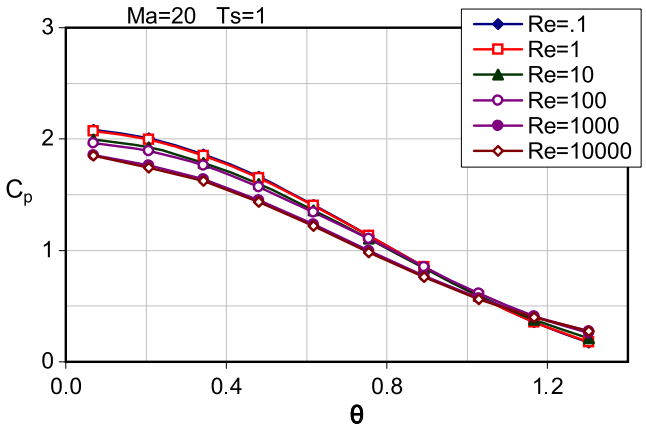

Fig. 7 (Color online) Pressure coefficient at ogive apex for diatomic gas (N_2), $\mathsf{Ma} = 20$, $T_s/T_\infty = 1$

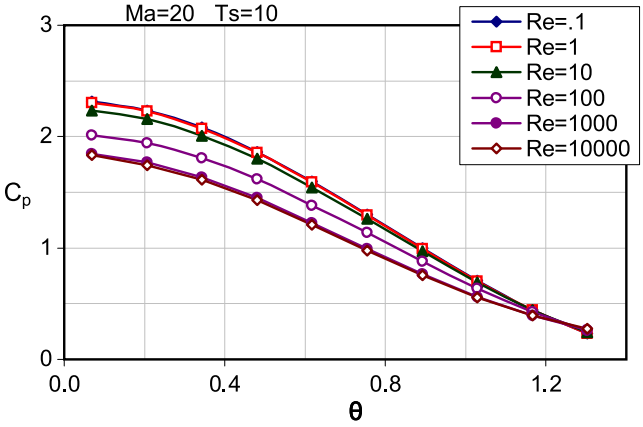

Fig. 8 (Color online) Pressure coefficient at ogive apex for diatomic gas (N_2), Ma = 20, $T_s/T_\infty = 10$

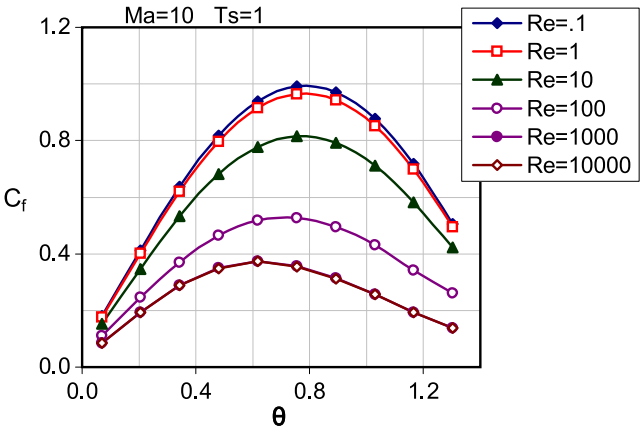

Fig. 9 (Color online) Friction coefficient, C_f, at ogive apex for diatomic gas (N_2), Ma = 10, $T_s/T_\infty = 1$

Mach numbers. The influence of the satellite temperature on C_p is negligible in the hydrodynamic regime (Re = 10,000) for both Mach numbers.

In the free-molecule regime (Re = 0.1) the satellite temperature weakly affects C_p at the higher Mach number (Ma = 20). The effect is more visible at Ma = 10.

C_p is maximum at the front part of the satellite ($\theta \approx 0$). Table 3 shows how C_p at this point depends on the Mach number and satellite temperature for both monatomic and diatomic gases. In the hydrodynamic range (Re > 1,000), the pressure coefficient for a diatomic gas is 2% to 3% larger than the coefficient for a monatomic gas.

4.4 Friction Coefficient

Figures 9, 10, 11, and 12 present the friction coefficient C_f as a function of the angle θ at Mach numbers 10 and 20, respectively, for the diatomic gas. The dependence

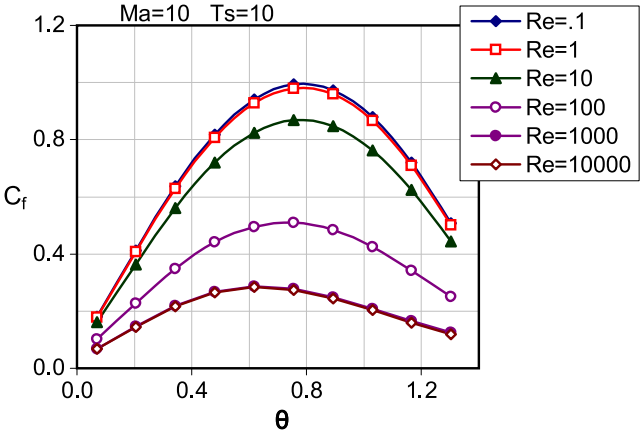

Fig. 10 (Color online) Friction coefficient, C_f, at ogive apex for diatomic gas (N_2), Ma = 10, $T_s/T_\infty = 10$

Table 3 Numeric values of pressure coefficient, C_p, at ogive apex near $\theta \approx 0$ for monatomic and diatomic gases

Ma	Re	Monatomic		Diatomic	
		$\frac{T_s}{T_\infty} = 1$	$\frac{T_s}{T_\infty} = 10$	$\frac{T_s}{T_\infty} = 1$	$\frac{T_s}{T_\infty} = 10$
10	0.1	2.189	2.645	2.190	2.646
	1	2.162	2.625	2.164	2.624
	10	2.031	2.454	2.035	2.456
	100	1.926	1.989	1.929	1.994
	1,000	1.776	1.764	1.823	1.796
	10,000	1.766	1.756	1.822	1.794
20	0.1	2.086	2.314	2.085	2.314
	1	2.071	2.306	2.071	2.305
	10	1.992	2.232	1.996	2.234
	100	1.965	2.008	1.964	2.011
	1,000	1.821	1.822	1.855	1.847
	10,000	1.803	1.797	1.851	1.835

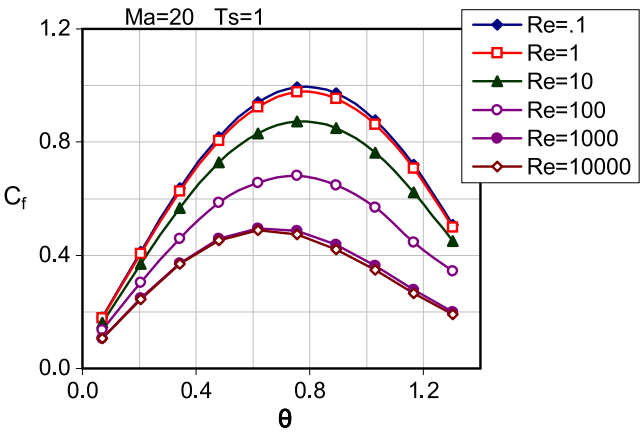

Fig. 11 (Color online) Friction coefficient, C_f, at ogive apex for diatomic gas (N_2), Ma = 20, $T_s/T_\infty = 1$

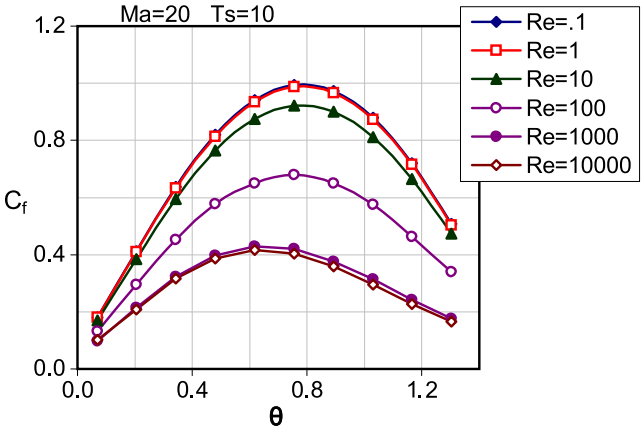

Fig. 12 (Color online) Friction coefficient, C_f, at ogive apex for diatomic gas (N_2), Ma = 20, $T_s/T_\infty = 10$

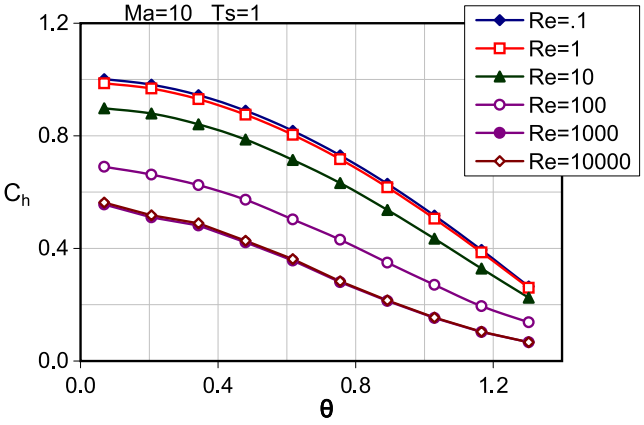

Fig. 13 (Color online) Energy transfer coefficient, C_h, at ogive apex for diatomic gas (N_2), Ma = 10, $T_s/T_\infty = 1$

on the Reynolds number Re highlights the effects of rarefaction. The steep rise in C_f as Re indicates that the friction coefficient is sensitive to gas rarefaction.

For high Re, the friction coefficient is also sensitive to changes in the Mach number. For Re = 10,000, relative to C_f at Ma = 10, the friction coefficient is nearly 30% higher for the "cold" satellite and 45% higher for the "hot" satellite. By contrast, at low Reynold numbers, the coefficient is practically independent of the Mach number.

At fixed Ma, in the free-molecule regime (Re = 0.1), the friction coefficient is likewise insensitive to changes in the satellite temperature. In the hydrodynamic regime (Re ≥ 1,000), the coefficient does depend on the satellite temperature: The maximum C_f for the "hot" satellite is 15% to 20% larger than the maximum for the "cold" one.

The maximum friction coefficient is in the vicinity of $\theta = \pi/4$. Table 4 lists values of C_f at this point for various Reynolds and Mach numbers, for both monatomic and diatomic gases. Again, the dependences on the Mach number and satellite temperature are weak in the free-molecule regime and stronger the hydrodynamic regime. While the C_f coefficient tends to be a little larger for the diatomic gas, the differences between the results for the monatomic and diatomic gas become noticeable only when the "cold" satellite is in the hydrodynamic regime at the higher Mach number.

Table 4 Numerical values of friction coefficient, C_f, at ogive apex near $\theta = \pi/4$ for monatomic and diatomic (N_2) gases

Ma	Re	Monatomic		Diatomic	
		$\frac{T_s}{T_\infty} = 1$	$\frac{T_s}{T_\infty} = 10$	$\frac{T_s}{T_\infty} = 1$	$\frac{T_s}{T_\infty} = 10$
10	0.1	0.992	0.994	0.992	0.994
	1	0.964	0.980	0.965	0.980
	10	0.811	0.867	0.817	0.868
	100	0.518	0.507	0.527	0.510
	1,000	0.333	0.273	0.356	0.278
	10,000	0.329	0.270	0.355	0.275
20	0.1	0.993	0.994	0.993	0.994
	1	0.975	0.987	0.976	0.987
	10	0.867	0.921	0.874	0.923
	100	0.673	0.674	0.681	0.679
	1,000	0.455	0.407	0.486	0.420
	10,000	0.432	0.383	0.473	0.404

4.5 Energy Transfer Coefficient

Figures 13, 14, 15, and 16 show that the energy transfer coefficient C_h as a function of θ is for a diatomic gas in for $T_s/T_\infty = 1$ ("cold" satellite) and $T_s/T_\infty = 10$ ("hot" satellite). C_h is very sensitive to changes in the Reynolds number (Re): It grows with rarefaction, i.e., as Re decreases. The dependence on the Mach number

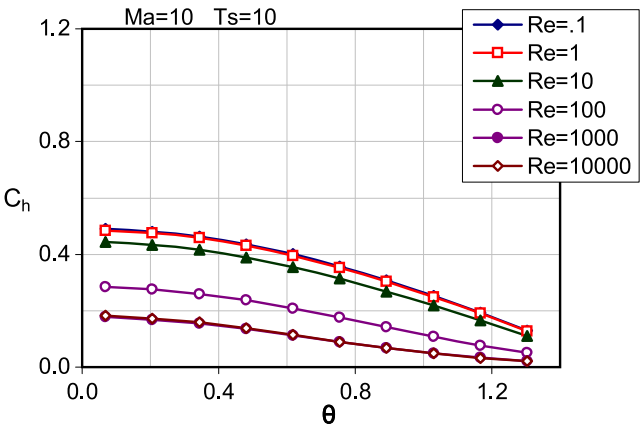

Fig. 14 (Color online) Energy transfer coefficient, C_h, at ogive apex for diatomic gas (N_2), Ma = 10, $T_s/T_\infty = 10$

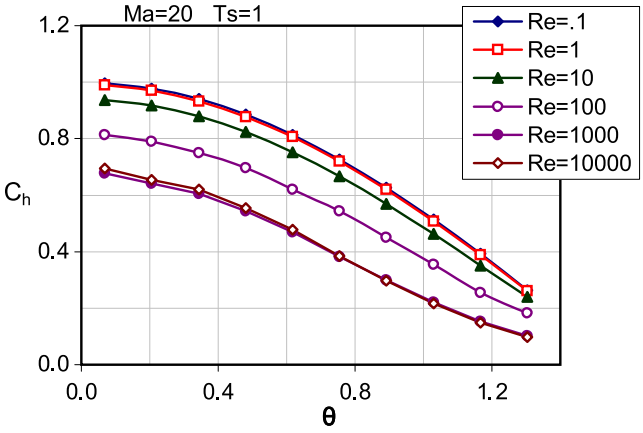

Fig. 15 (Color online) Energy transfer coefficient, C_h, at ogive apex for diatomic gas (N_2), Ma = 20, $T_s/T_\infty = 1$

Table 5 Numerical values of energy transfer coefficient, C_h, at ogive apex near $\theta = \pi/4$ for monatomic and diatomic (N_2) gases

Ma	Re	Monatomic		Diatomic	
		$\frac{T_s}{T_\infty} = 1$	$\frac{T_s}{T_\infty} = 10$	$\frac{T_s}{T_\infty} = 1$	$\frac{T_s}{T_\infty} = 10$
10	0.1	1.001	0.490	1.001	0.490
	1	0.986	0.485	0.987	0.485
	10	0.895	0.444	0.898	0.443
	100	0.676	0.286	0.690	0.285
	1,000	0.489	0.173	0.556	0.179
	10,000	0.492	0.179	0.563	0.183
20	0.1	0.996	0.869	0.996	0.869
	1	0.989	0.865	0.989	0.865
	10	0.934	0.831	0.937	0.831
	100	0.803	0.679	0.813	0.682
	1,000	0.617	0.477	0.678	0.507
	10,000	0.634	0.492	0.696	0.522

is weak for the "cold" satellite and stronger for the "hot" satellite.

C_h is maximum at the frontal point of the satellite ($\theta = 0$). Table 5 shows C_h at this point for the monatomic and diatomic gases and various combinations of Re, Ma, and T_s/T_∞.

Compared to the "cold" satellite, the "hot" satellite exhibits similar energy transfer coefficients at the higher Mach number (Ma = 20). At the lower Mach number (Ma = 10), however, C_h changes substantially with temperature: The ratio between the coefficients for the "cold" and the "hot" satellites is particularly large in the hydrodynamical regime, the diatomic gas yielding larger C_h's than the monatomic gas.

4.6 Density Distribution

Figures 17, 18, 19, and 20 show the density distribution ρ/ρ_∞ in the space surrounding the "cold" satellite at Ma = 20 for the diatomic gas in the three flow regimes: free molecule, transition, and hydrodynamic. At Ma = 10, the density distribution qualitatively has the same behavior and is very similar to the distribution for a monatomic gas. The density distribution pattern is also insensitive to changes in the satellite temperature.

Particularly evident in the figures is the qualitative change in the flow pattern as the Reynolds number is decreased. This evolution reflects the progressive reduction in the interaction between flow particles, i.e., collisions between gas molecules, as the gas becomes more rarefied at low Reynolds number.

In the free-molecule regime, in the absence of interparticle interaction, only the collisions with the satellite surface can change the trajectories of the particles. A shadow (vacuum) with a well-defined boundary parallel to the flow is clearly visible in the downstream region close to the base of satellite, where practically no particles from the upstream flow can be found.

In the transition regime, the frequency of collisions between particles increases, and the interaction

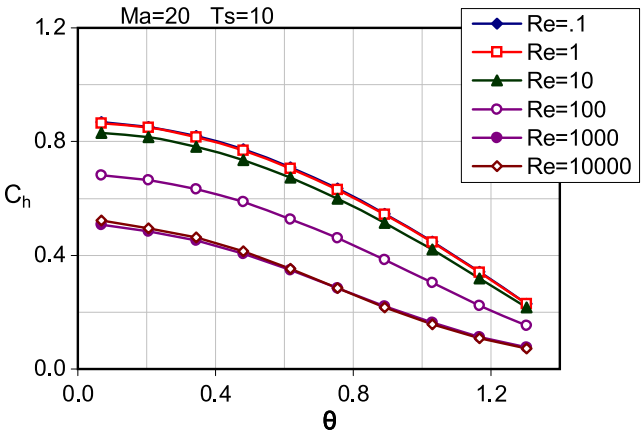

Fig. 16 (Color online) Energy transfer coefficient, C_h, at ogive apex for diatomic gas (N_2), Ma = 20, $T_s/T_\infty = 10$

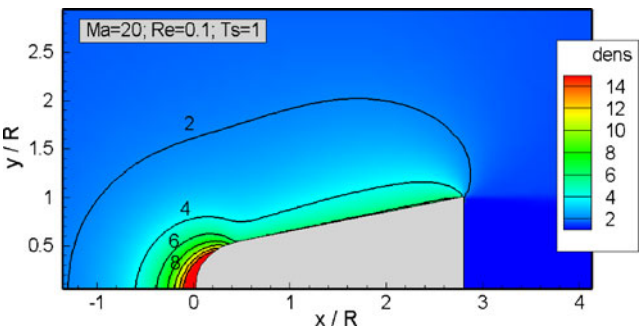

Fig. 17 (Color online) Density distribution, ρ/ρ_∞, in the free molecule regime for a "cold" satellite (Ma = 20, Re = 0.1, $T_s/T_\infty = 1$)

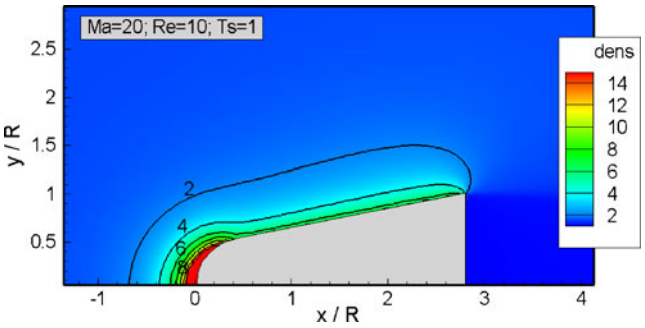

Fig. 18 (Color online) Density distribution, ρ/ρ_∞, in the transition regime for a "cold" satellite (Ma = 20, Re = 10, $T_s/T_\infty = 1$)

between the oncoming flow and reflected particles becomes noticeable as the region of inhomogeneous density narrows and acquires a more distinct boundary. Finally, in the hydrodynamical regime, the region of inhomogeneous density becomes well delimited by a bow (detached) shock wave.

4.7 Temperature Distribution

Figures 21, 22, 23, and 24 show the temperature distribution T/T_∞ in the space surrounding the "cold" satellite for Ma = 20 and a diatomic gas in the three flow regimes: free molecule, transition, and hydrodynamic. The temperature distribution at Ma = 10 is qualitatively the same, and practically no differences are found when a monatomic gas is substituted for the diatomic gas. Likewise, the temperature distributions around a "hot" satellite are very similar.

The temperature distribution clearly shows the qualitative difference between the three flow regimes. In the hydrodynamic regime (Re = 10,000), the bow shock in front of the satellite is easily recognized; with increasing rarefaction (Re = 100 and 10–transition regime) the shock moves away from the satellite and

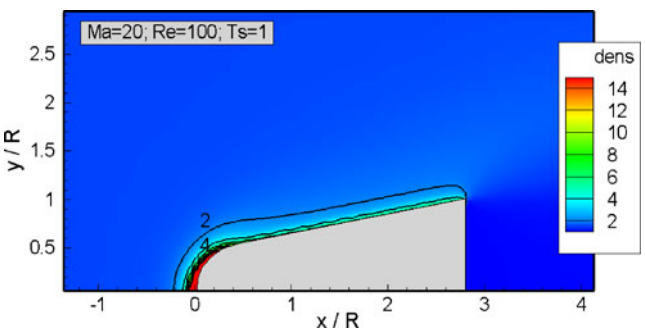

Fig. 19 (Color online) Density distribution, ρ/ρ_∞, in the transition regime for a "cold" satellite (Ma = 20, Re = 100, $T_s/T_\infty = 1$)

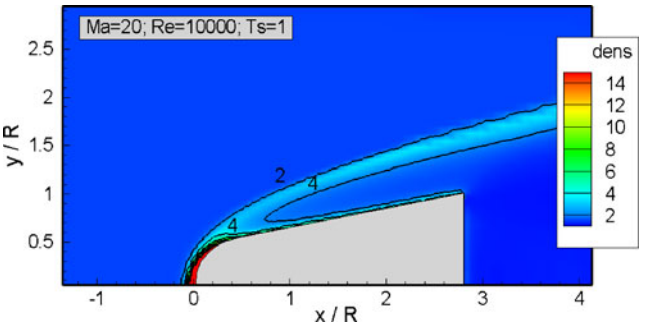

Fig. 20 (Color online) Density distribution, ρ/ρ_∞, in the hydrodynamic regime for a "cold" satellite (Ma = 20, Re = 10,000, $T_s/T_\infty = 1$)

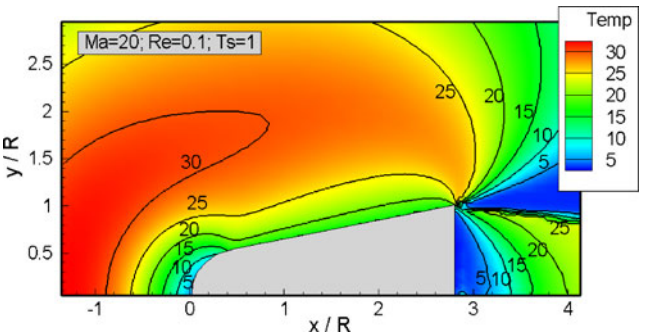

Fig. 21 (Color online) Temperature distribution, T/T_∞, in the free molecule regime for a "cold" satellite (Ma = 20, Re = 0.1, $T_s/T_\infty = 1$)

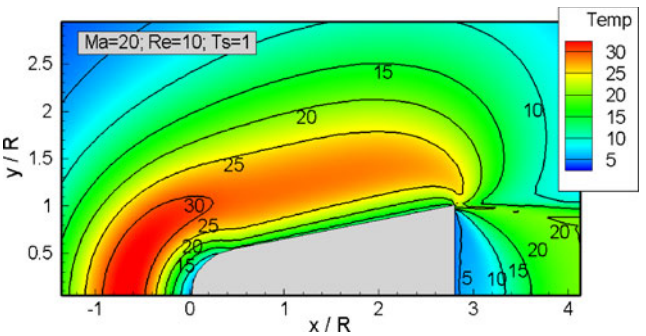

Fig. 22 (Color online) Temperature distribution, T/T_∞, in the transition regime for a "cold" satellite (Ma = 20, Re = 10, $T_s/T_\infty = 1$)

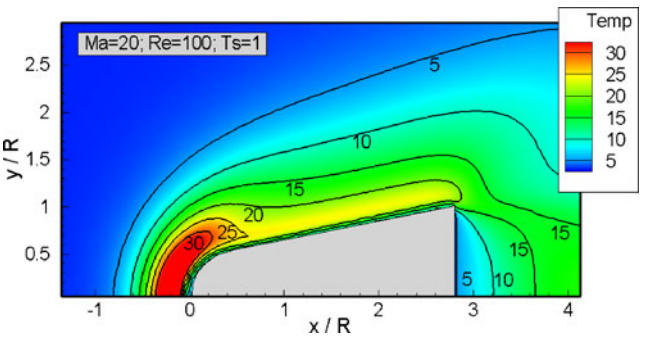

Fig. 23 (Color online) Temperature distribution, T/T_∞, in the transition regime for a "cold" satellite (Ma = 20, Re = 100, $T_s/T_\infty = 1$)

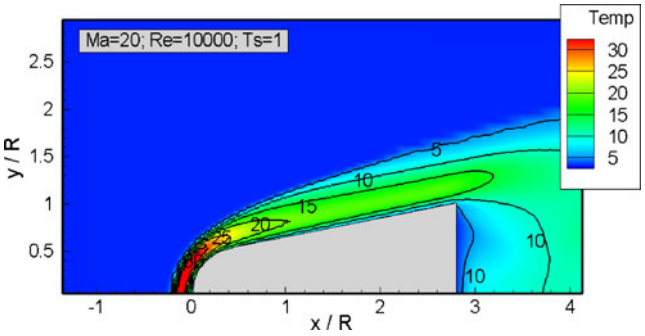

Fig. 24 (Color online) Temperature distribution, T/T_∞, in the hydrodynamic regime for a "cold" satellite (Ma = 20, Re = 10,000, $T_s/T_\infty = 1$)

becomes less defined. In the free molecule regime (Re = 0.1), it disappears.

The flow patterns at the two Mach numbers (Ma = 10 and 20) are qualitatively the same, but the temperature and its gradients are larger for the larger Mach number. For Ma = 10, the temperatures in the frontal region of the satellite are roughly ten times higher than the temperature T_∞ of the unperturbed flow. At Ma = 20, the ratio is close to 100.

4.8 Local Mach Number Distribution

Figures 25, 26, 27, and 28 show the distribution of the local Mach number Ma_L in the space surrounding the "cold" satellite for Ma = 20 and a diatomic gas in the three flow regimes: free molecule, transition, and hydrodynamic. The flow streamlines are shown in Figs. 29, 30, 31, and 32.

In the hydrodynamic regime (Re = 10,000), the Mach number drops very sharply across the boundary of the shock wave, due to the strong effect of viscosity in this regime and to the presence of vorticity in the base region of satellite. In the free molecule regime, the

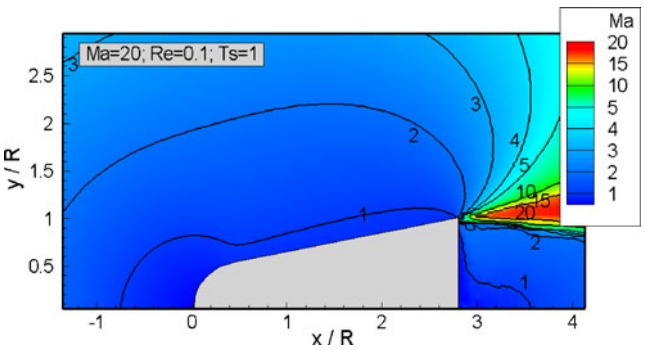

Fig. 25 (Color online) Local Mach distribution, Ma_L, in the free molecule regime for a "cold" satellite (Ma = 20, Re = 0.1, $T_s/T_\infty = 1$)

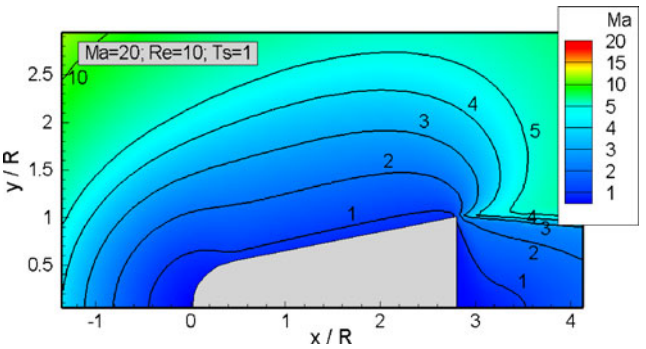

Fig. 26 (Color online) Local Mach distribution, Ma_L, in the transition regime for a "cold" satellite (Ma = 20, Re = 10, $T_s/T_\infty = 1$)

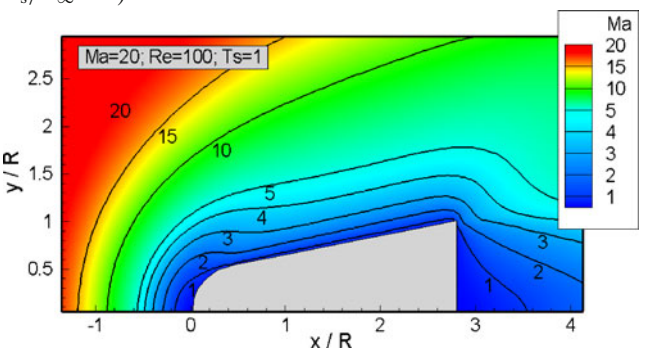

Fig. 27 (Color online) Local Mach distribution, Ma_L, in the transition regime for a "cold" satellite (Ma = 20, Re = 100, $T_s/T_\infty = 1$)

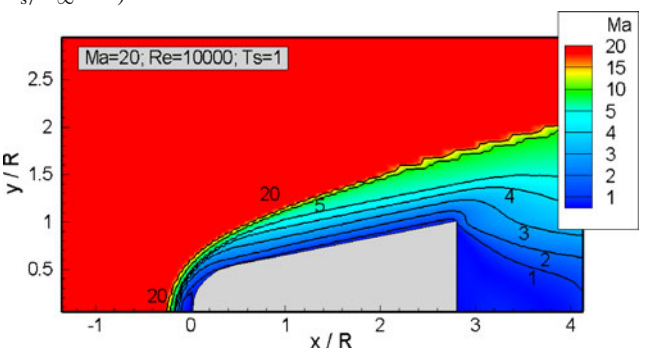

Fig. 28 (Color online) Local Mach distribution, Ma_L, in the hydrodynamic regime for a "cold" satellite (Ma = 20, Re = 10,000, $T_s/T_\infty = 1$)

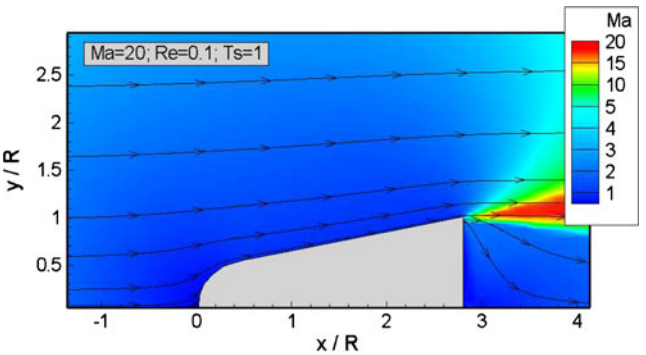

Fig. 29 (Color online) Streamlines in the free molecule regime for a "cold" satellite (Ma = 20, Re = 0.1, $T_s/T_\infty = 1$)

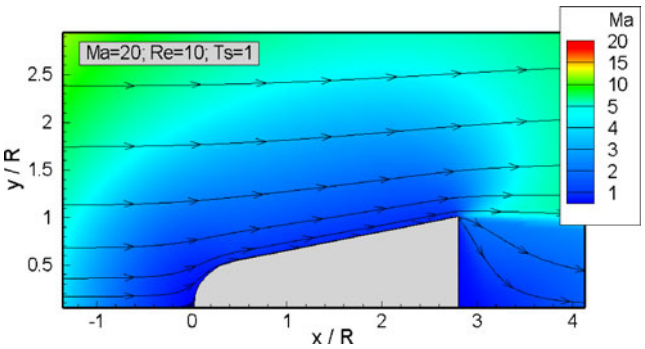

Fig. 30 (Color online) Streamlines in the transition regime for a "cold" satellite (Ma = 20, Re = 10, $T_s/T_\infty = 1$)

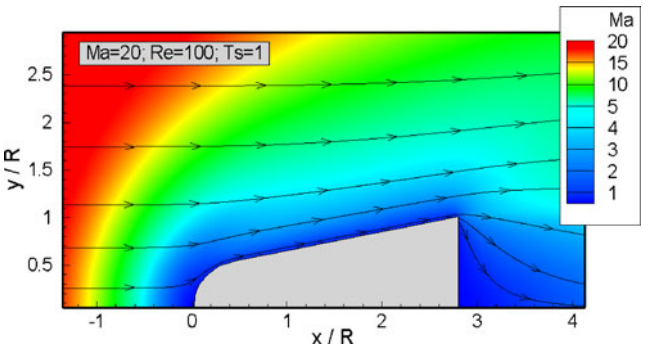

Fig. 31 (Color online) Streamlines in the transition regime for a "cold" satellite (Ma = 20, Re = 100, $T_s/T_\infty = 1$)

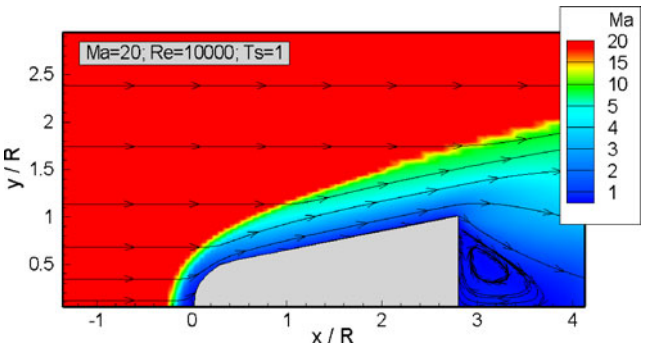

Fig. 32 (Color online) Streamlines in the hydrodynamic regime for a "cold" satellite (Ma = 20, Re = 10,000, $T_s/T_\infty = 1$)

local Mach number distribution is completely different from the distribution for the hydrodynamic regime due inexistence of interaction between gaseous particles. The pattern for the "hot" satellite is very similar to the one in Figs. 29, 30, 31, and 32.

5 Concluding Remarks

The DSMC was used to calculate the characteristics of gas flow around a satellite during an orbital and reentry flight. The drag coefficient was determined together with the pressure, friction, and energy transfer coefficients over the satellite surface. The distributions of density, temperature, and local Mach number of the flow surrounding the satellite were also computed. The computations were based on the physical properties of nitrogen, N_2, which is the main constituent of the atmosphere.

Significant differences distinguish the interactions between flow particles and between particles and surface in a diatomic gas from those in a monatomic substance. In a monatomic gas, the collisions are elastic and only translational energy can be exchanged. In polyatomic gases, the exchange involves internal degrees of freedom, such as the rotational and vibrational modes. The collisions between particles and between particles and surfaces are no longer elastic. The Larsen–Borgnakke model was used to account for such interactions, and the variable hard sphere molecular model, which is appropriate to describe polyatomic gases, was adopted to describe intermolecular collisions.

Qualitatively, our results are very close to those for a monatomic gas. When the coefficients calculated for the diatomic gas are compared with the coefficients for the monatomic gas, as summarized in Tables 6 and 7,

Table 6 Summary of relative differences between flow parameters calculated for monatomic and diatomic gases, Ma = 10

ΔPar.	$\Delta\text{Par.} = (\text{Par.})_{\text{Diat.}} - (\text{Par.})_{\text{Monat.}}$			
	$\frac{T_s}{T_\infty}$	Regime		
		Free Mol. (%)	Trans. (%)	Hydrod. (%)
ΔC_D	1	0	–1	0
	10	0	–1	0
ΔC_p ($\theta \approx 0$)	1	0	0	3
	10	0	0	2
ΔC_f ($\theta \approx \pi/4$)	1	0	1	7
	10	0	0	2
ΔC_h ($\theta \approx 0$)	1	0	1	14
	10	0	0	3

Table 7 Summary of relative differences between flow parameters calculated for monatomic and diatomic gases, Ma = 20

ΔPar.	$\Delta\text{Par.} = (\text{Par.})_{\text{Diat.}} - (\text{Par.})_{\text{Monat.}}$			
	$\frac{T_s}{T_\infty}$	Regime		
		Free Mol. (%)	Trans. (%)	Hydrod. (%)
ΔC_D	1	0	–1	–2
	10	0	–1	–3
ΔC_p ($\theta \approx 0$)	1	0	0	2
	10	0	0	2
ΔC_f ($\theta \approx \pi/4$)	1	0	1	8
	10	0	1	4
ΔC_h ($\theta \approx 0$)	1	0	1	10
	10	0	0	6

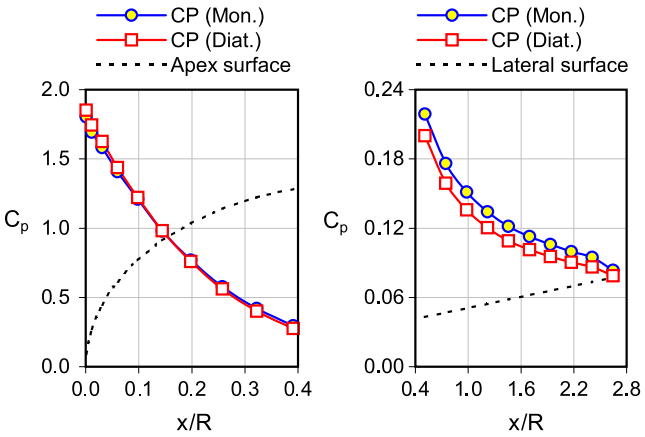

Fig. 33 Distribution of pressure coefficient, C_p, over satellite surface for $\mathrm{Ma} = 20$, $T_s/T_\infty = 1$ and $\mathrm{Re} = 10{,}000$ (monatomic and diatomic gas—hydrodynamic regime)

negligible differences are seen in the free-molecule regime, very small ones are found in the transition regime, and greater distinctions arise in the hydrodynamic regime.

In the hydrodynamic sections of the two tables, the drag and pressure coefficients C_D and C_p are less sensitive to the adopted model, while the friction and energy transfer coefficients C_f (for $\theta \approx \pi/4$) and C_h (for $\theta \approx 0$) are more sensitive. In any case, the relative differences are inferior to 10%. In the hydrodynamic regime, the influence of the satellite temperature is significant only for the friction and energy transfer coefficients.

Comparison between the hydrodynamic regimes for the diatomic and the monatomic gases shows that the drag coefficient C_D is smaller for the diatomic gas, while ΔC_p ($\theta \approx 0$) and ΔC_f ($\theta \approx \pi/4$) is larger for the monatomic gas. This would seem contradictory.

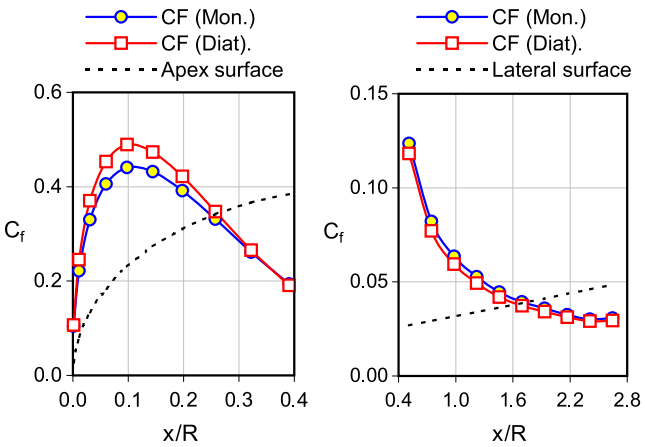

Fig. 34 Distribution of friction coefficient, C_f, over satellite surface for $\mathrm{Ma} = 20$, $T_s/T_\infty = 1$ and $\mathrm{Re} = 10{,}000$ (monatomic and diatomic gas—hydrodynamic regime)

Nonetheless, as Figs. 33 and 34 show, at the ogive apex, the pressure and friction coefficients are larger for the diatomic gas, but in the lateral part of the satellite, the monatomic gas yields the dominant coefficients. Due to this inversion, the final integration of the horizontal components of the two coefficients (which contributes to the drag coefficient) over the satellite surface in the x direction results in a lower C_D for the diatomic gas (a small decrease of the order of 1% to 2% in this case).

We conclude that the monatomic gas model describes accurately the flow in the free-molecule and transition regimes. More significant are the differences between the monatomic and diatomic gases in the hydrodynamic regime. Even here, however, only the differences between the friction and energy transfer coefficients are significant, the coefficients being higher for the diatomic gas.

Acknowledgements One of the authors (F.Sh.) acknowledges the Conselho Nacional de Desenvolvimento Científico e Tecnológico (CNPq, Brazil) for the support of his research. Partially, the present calculations were carried out at the Laboratório Central de Processamento de Alto Desempenho (LCPAD) of UFPR, Brazil.

References

1. M.N. Kogan, Prog. Aerosp. Sci. **29**, 271 (1992)
2. D.F.G. Rault, J. Spacecr. Rockets **31**(6), 944 (1994)
3. F. Sharipov, Braz. J. Phys. **33**(2), 398 (2003)
4. F. Sharipov, in *Rarfeid Gas Dynamics*, ed. by A. Ketsdever, E.P. Muntz. 23rd Int. Symp., Canada, 2002, vol. 663 (American Institute of Physics, Melville, 2003), pp. 1049–1056
5. G.N. Markelov, A.N. Kudryavtsev, M.S. Ivanov, in *Rarefied Gas Dynamics*, ed. by R. Brun, R. Campargue, R. Gatignol, J.C. Lengrand. 21st Int. Symp., France, 1998, vol. 2 (CEPAD, Toulouse, 1999), pp. 647–654
6. M.N. Kogan, *Rarefied Gas Dynamics* (Plenum, New York, 1969)
7. C. Cercignani, *The Boltzmann Equation and its Application* (Springer, New York, 1988)
8. C. Cercignani, *Theory and Application of the Boltzmann Equation* (Scottish Academic, Edinburgh, 1975)
9. J.H. Ferziger, H.G. Kaper, *Mathematical Theory of Transport Processes in Gases* (North-Holland, Amsterdam, 1972)
10. F. Sharipov, V. Seleznev, J. Phys. Chem. Ref. Data **27**(3), 657 (1998)
11. G.A. Bird, *Molecular Gas Dynamics and the Direct Simulation of Gas Flows* (Oxford University Press, Oxford, 1994)
12. F. Sharipov, in *West East High Speed Flow Fields* (Int. Conf., 2005), pp. 507–512
13. A.V. Nakarjakov, S.F. Borisov, F.M. Sharipov, P.E. Suetin, in *Rarefied Gas Dynamics*, ed. by B.D. Shizgal, D.P. Weaver. 19th Int. Symp., vol. 2 (Oxford University Press, Oxford, 1995), pp. 954–959
14. O.V. Sazhin, S.F. Borisov, F. Sharipov, J. Vac. Sci. Technol. A **19**(5), 2499 (2001). Erratum: **20**(3), 957 (2002)
15. C. Shen, *Rarefied Gas Dynamics. Fundamentals, Simulations and Micro Flows* (Springer, Berlin, 2005)